JOURNAL OF THERMOPHYSICS AND HEAT TRANSFER
Vol. 19, No. 4, October–December 2005

# Experimental Study of a Reversible Loop Heat Pipe

Bong-Hun Kim*
*Daegu University, Jinryang, Kyungbuk 712-714, Republic of Korea*
and
G. P. Peterson†
*Rensselaer Polytechnic Institute, Troy, New York 12180*

**An experimental investigation of a reversible loop heat pipe was conducted to determine the operating limits and performance characteristics as a function of the thermophysical and geometric parameters, the heat input, and the cooling intensity. Variations in both the temperature and heat transport capacity were measured and analyzed to accurately evaluate the transient operating characteristics. In addition, the maximum heat transport as a function of the mean evaporator temperature, the ratio of heat transport to heater input power as a function of the mean evaporator temperature, and the overall thermal resistance as a function of the overall heat transport capacity were examined. The results indicated that the operating limits and performance characteristics of these devices were a strong function of the cooling intensity, with the maximum heat transport corresponding to a cooling intensity of 290 W/°C, more than twice that obtained for a cooling intensity of 72 W/°C. Observation of the transient startup characteristics indicated that the optimal mean evaporator temperature for reliable startup was in the range of 35 to 60°C. Using these operating parameters, overall thermal resistances as low as 0.02°C/W were measured.**

## Nomenclature

| | | |
|---|---|---|
| $c_p$ | = | specific heat, J/kg · °C |
| $E_{\mathrm{st},c}$ | = | rate of change of energy in the condenser, W |
| $E_{\mathrm{st},e}$ | = | rate of change of energy in the evaporator, W |
| $h_l$ | = | liquid enthalpy, J/kg |
| $h_v$ | = | vapor enthalpy, J/kg |
| $k_{\mathrm{eff}}$ | = | effective thermal conductivity, W/m · K |
| $\dot{m}_c$ | = | coolant mass flow rate, kg/s |
| $\dot{m}_l$ | = | liquid mass flow rate, kg/s |
| $\dot{m}_v$ | = | vapor mass flow rate, kg/s |
| $mcp$ | = | cooling intensity, W/°C |
| $P$ | = | pressure, MPa |
| $q_i$ | = | heat input, W |
| $q_{L,c}$ | = | heat loss from the condensor, W |
| $q_{L,e}$ | = | heat loss from the evaporator, W |
| $R$ | = | thermal resistance, °C/W |
| $T_{\mathrm{ci}}$ | = | coolant inlet temperature, °C |
| $T_{\mathrm{co}}$ | = | coolant outlet temperature, °C |
| $T_{c,m}$ | = | average condenser temperature, °C |
| $T_{e,m}$ | = | average evaporator temperature, °C |
| $V_h$ | = | output voltage of power transducer, V |
| $V_m$ | = | output voltage of mass flow meter, V |

*Subscripts*

| | | |
|---|---|---|
| $c$ | = | coolant or condenser |
| $e$ | = | evaporator |
| $h$ | = | heater |
| $i$ | = | inlet or input |
| $L$ | = | heat loss |
| $m$ | = | mass flow rate or average value |
| $o$ | = | exit |
| $s$ | = | sensible heat |
| st | = | energy storing |
| $w$ | = | wick |

Received 30 October 2004; revision received 16 January 2005; accepted for publication 19 January 2005. 

*Associate Professor, Automotive, Industrial, and Mechanical Engineering Department.
†Professor and Provost, Mechanical, Aerospace, and Nuclear Engineering Department. Fellow AIAA.

## I. Introduction

LOOP heat pipes (LHPs) are similar to traditional heat pipes in that they utilize a two-phase heat transfer process resulting in minimal temperature drops. As is the case for conventional heat pipes, LHPs utilize the capillary forces inherent in a wicking structure to pump a working fluid from the heat source to the heat sink. Heat applied to the evaporator is conducted through the evaporator wall, resulting in evaporation of the working fluid, which results in evaporation of the saturated liquid. The vapor then flows to the condenser through the vapor transport line. At the condenser, heat is rejected and the vapor condensed, causing the vapor to give up the latent heat, which is rejected to the outer surface of the condenser. The liquid flowing out of the two-phase region of the condenser enters a subcooler or compensation chamber, which is serially connected to the end of the condenser and designed to eliminate vapor bubbles by providing sufficient subcooling to the liquid. Finally, the subcooled liquid returns to the evaporator due to the capillary pressure gradient, completing the thermal loop.

In addition to the high capillary pressure generated by the wicking structure, an important feature of an LHP is the separation of the liquid and vapor flows into separate flow lines. This makes it possible to significantly reduce liquid-side pressure loss as well as removing the interfacial instabilities frequently occurring at the flooded wick surface. The combination of high capillary pressures and low frictional pressure drops results in a relatively high heat transport limit, even when the condenser and evaporator are separated over distances of up to 3 m or more. Using ultrafine porous metal powder wicks, heat transport limits as high as 1.7 kW have been observed.[1]

Because of the high capillary pumping pressure and low frictional pressure drop, these devices are best applied in situations involving very high heat loads over long distances, or in adverse gravitational environments.[2] In addition, because of the possibility of utilizing flexible liquid and vapor transport lines, these devices are well suited for use in deployable spacecraft radiators.[3] Previous investigations have determined that LHPs can satisfy the rigorous operational requirements even for advanced spacecraft and these devices have been selected as one of several candidate thermal control systems for the Earth Observing System[4] and as part of the baseline design for the thermal control systems for NASA's Geoscience Laser Altimeter Systems.[5]

The first investigations of LHPs were related to capillary-driven steam generators developed by Laub and McGinness[6] and McGinness[7] at the end of 1950s. In the middle of the 1960s, the proof-of-concept tests were first conducted by Stenger[8] at the NASA Lewis Research Center. In this investigation, the overall operating characteristics and heat transport limits were evaluated using a test article capable of transporting more than 800 W over distances of 1.5 m. Over the next 20 years, work focused on more traditional heat pipes and very little information on LHPs is available in the literature. However, because of the limitation of more traditional heat pipes, extensive research on LHPs resumed in the mid-1980s, and the advantages of these devices for applications in advanced thermal control systems were newly recognized.

The basic concepts and operating principles of LHPs designed for use in the thermal control of spacecraft was presented in the first patent issued to Maidanik et al.[9] Expanding on the initial concept introduced by Stenger,[8] a test article (model LA-ITF-07) was manufactured by the Lavochkin Scientific and Production Association and the initial test results were reported by Maidanik et al.[10] Shortly thereafter, proof-of-concept tests using an ammonia LHP were performed by Dickey and Peterson[11] to verify the overall transport capacity and to better understand the operational characteristics. In this investigation, the evaporator and condenser were approximately 120 mm long, had an outer diameter of 12 mm, and were constructed using stainless steel tubes with a porous metal wick inserted in the evaporator. Results of these tests indicated a maximum heat transport and overall thermal resistance of 130 W and 0.15°C/W, respectively.

Numerous additional theoretical and experimental investigations were conducted during the late 1990s and significant progress was observed in the modeling and experimental test methods.[12–16] Kaya and Hoang[5] presented a mathematical model of the LHP, which was validated by experiments performed for sintered nickel wicks with pore sizes of 1.2 $\mu$m and ammonia as a working fluid. A separate subcooler with no additional wick was installed at the outlet of the condenser. Two test articles were developed. LHP1 had a cylindrical evaporator with a diameter of 25.4 mm and a length of 150 mm. A compensation chamber having a diameter of 46 mm and a length of 76 mm was connected to the evaporator. The total length was not clearly indicated in the study, but was estimated to be approximately 1000 mm. The evaporator and compensation chambers of LHP2 were designed to be twice as long as those for LHP1 but had similar diameters. The overall length was 2032 mm. The study reported that the model prediction was very accurate at steady state. It was also suggested that physical mechanisms of the LHP should be investigated more widely to fully understand the temperature hysteresis and the transient effects.[5] Although this and other work was useful in understanding the basic operating principles, there were very few innovative design concepts that would fully satisfy the requirements for space applications.

At the end of the 1990s, new requirements for a number of thermal control devices for use in spacecraft emerged. These requirements included the ability of these devices to operate equally well in either direction, thereby eliminating the thermal diode effect commonly observed in most of the previously designed LHPs.[17] In addition to the previous requirements, such as high heat transport capability, low payload, and flexible structure, this option has become an important issue when considering the periodically changing environmental conditions and the relative position of spacecraft with respect to the sun.

In this sense, a new design, called a reversible loop heat pipe (RLHP), was proposed by Maidanik.[18] The RLHP was designed to enable heat transfer equally well in both directions. The key component of this new design was an ultrafine metal wick, with pore sizes of 1.1 $\mu$m and a porosity of 67%, which was designed for use in both the evaporator and the condenser to obtain high heat transport capability in both directions.

## II. Experimental Apparatus and Procedure

The objectives of the current investigation are to test and evaluate the operating characteristics and performance limitations of these RLHPs in a horizontal orientation, with ammonia as a working fluid. The tests were conducted for a range of operating temperatures, heat inputs, and cooling intensities. First, the average evaporator and condenser temperatures as well as the heat transport ratio (defined as the ratio of heat transport to heat input) were measured to evaluate the transient response characteristics of the RLHP. Second, the heat transport limit and overall thermal resistance were measured at steady state for the given heat input and cooling intensity.

### A. Configuration and Operation Principles of RLHP

Figure 1 illustrates an internal schematic of the evaporator and condenser of the RLHP test article, which has the internal wicking design. As shown, the evaporator and condenser are approximately 190 mm long, have an external diameter of 24 mm, and are made of a stainless steel tube. To promote circumferential distribution of the working fluid and enhance the vaporization, triangular grooves, 0.14 mm wide and 0.15 mm deep, are machined on the inner wall of the tube. A porous metal wick fabricated from sintered nickel powder, with an effective pore size of 1.1 $\mu$m and a porosity of 67%, is inserted into the tube. This wick is 115 mm long with inner and outer diameters of 22 and 14 mm, respectively, and longitudinal rectangular grooves, 1 mm wide and 1 mm deep, at a pitch of 2 mm on the outer surface. An ungrooved compensation chamber is connected to the left-hand side of the tube as shown, and connects the evaporator and condenser by a liquid line.

The operating principles of traditional LHPs have been explained by Faghri,[2] and although the operation of RLHPs is similar, there are a number of significant differences. In RLHPs, heat is applied to the active zone of the evaporator (corresponding to the region with the metal wick inside, as shown in Fig. 1); vapor is generated from the liquid in the triangular circumferential grooves. All of the heat, with the exception of that conducted through the portion of the sintered wick contacting the stainless steel tube, contributes to the phase change. This heat results in vaporization from the concave liquid menisci of individual pores in the wicking structure. Flooding is retarded because the vapor pressure developed inside of the vapor space in the longitudinal grooves causes the liquid interface to recede into the wick pores. The vapor then flows through the vapor line to the condenser, where it is condensed on the inner surface of the stainless steel tube. In the condenser, the condensate collects in the circumferential grooves and is drawn into the porous wicking structure. As was the case in the evaporator, some phase change occurs in the porous wick close to the contact point between the wick and the stainless steel tube because of the heat conducted through the sintered wick. The liquid condensate absorbed into the wick is then forced thorough the wick and into the inner vacant core by the high vapor pressure, maintaining the full charge of the liquid return line.

The saturated liquid typically changes to a slightly subcooled state as it flows from the wick to the compensation chamber located in the left-hand side of the condenser. Under steady-state condition, the RLHP operating temperature is self-regulating, adjusting in such a way that the condenser generates sufficient subcooling to make up for the heat leakage and heat loss to the environment.[5] The subcooled liquid flows out of the active zone and accumulates in the

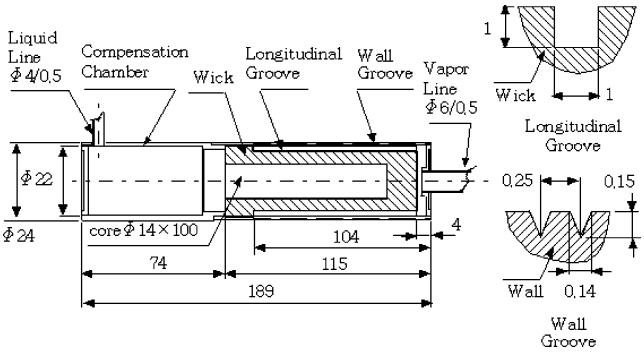


**Fig. 1 Detailed configuration of the RLHP evaporator/condenser.**

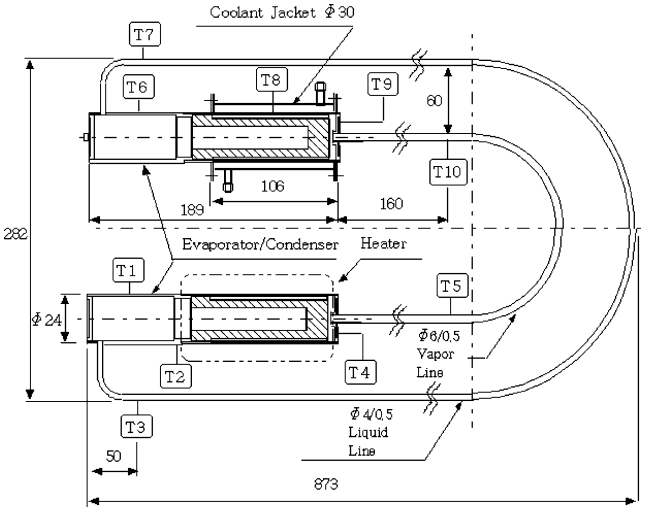


**Fig. 2 Configuration of the RLHP and location of the thermocouples.**

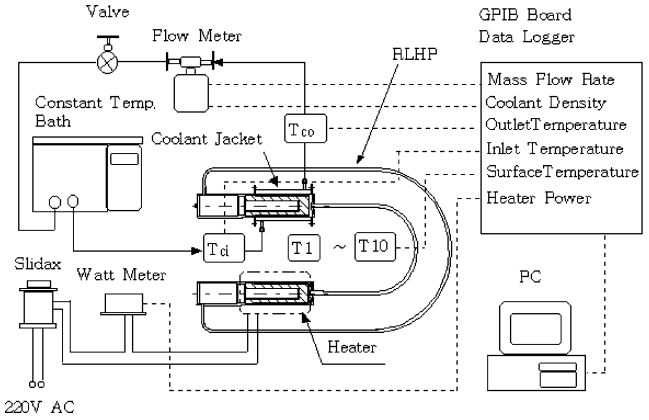


**Fig. 3 Schematic diagram of the experimental setup.**

compensation chamber, which serves as a reservoir designed to continuously absorb liquid as well as to adjust the degree of subcooling. As a result of the pressure difference between the evaporator and condenser, the subcooled liquid flows through the liquid line to the other compensation chamber of the evaporator.

The compensation chamber serves as a reservoir to continuously supply subcooled liquid to the evaporator as well as to regulate the flooding level of the wick interface. Boiling and/or phase change does not typically occur in this chamber, because the evaporator heaters are installed only on the portion of the surface in contact with the wick. As such, one of the important functions of the compensation chamber is that it can prevent or retard bubble generation, which usually causes severe degradation of performance, especially when the wick is flooded.

As the subcooled liquid flows through the active zone of the evaporator, shown in Fig. 1, it is vaporized and may boil if the superheat is too high. This boiling may at times become violent, leading to depriming of the wick due to the large fluctuations in the vapor pressure.[19] In addition, the degree of superheat may become larger as the pore size decreases, because lower liquid pressure is encountered due to greater pressure loss across the wick. However, violent boiling can be significantly retarded by increasing the degree of subcooling.[20] In the present study, which used an ultrafine wick, subcooling was a more important parameter in determining the operating characteristics and heat transport capacity than in conventional LHPs, particularly during startup, where there must be sufficient subcooling to provide the pressure difference required for the circulation of the working fluid.

As shown in Fig. 2, the total length of the RLHP evaluated here was approximately 2 m, but, during the tests, it was folded to an overall length of 873 mm. The evaporator and condenser were symmetrically positioned in the same horizontal plane and connected by two stainless steel tubes. In the evaporator, a 100-mm-long band heater was installed in the active zone, and, similarly, a concentric cooling jacket with an outer diameter of 30 mm and a length of 106 mm was placed in contact with the condenser. Ten T-type thermocouples were attached to the outer surface of the test article, three each in the evaporator and condenser and four in the vapor and liquid lines. These were placed as follows: T1 and T6 were located in the middle of the compensation chamber; T2 and T4 were placed on the outer surface close to the heater, to measure the evaporator temperature; and T8 and T9 were located in the middle of the cooling jacket and the right-hand side of the condenser, respectively, to measure the condenser temperature.

### B. Experimental Facility

Figure 3 illustrates the experimental setup, which consisted of the RLHP test article, the heating and cooling systems, and a computerized data acquisition system. The heating system utilized a 1200-W band heater, a manual transformer and a watt transducer to measure the power with analog output (1–5 V for 0–1200 W). The cooling system consisted of a constant-temperature bath, a mass flow meter, and a cooling jacket with RTD temperature probes. The constant-temperature bath supplied coolant with a 34% mass fraction of ethylene glycol, regulated at $10 \pm 0.1^{\circ}$C to the cooling jacket, which had two Chino, Pt100, A-class RTD temperature sensors. The mass flow meter was an Oval model D025S-SS/MT9739, installed at the outlet of the cooling jacket to measure the coolant mass flow rate with an analog output of 1–5 V over a range of 0 to 10 kg/min. The data logger was equipped with GPIB board connected to a personal computer. All of the measured data, including 10 surface temperatures, 2 coolant temperatures, and 2 analog outputs from the power transducer and mass flow meter, were recorded at 5-s intervals. During the experiment, the RLHP and the cooling and heating devices were tightly insulated and encased in a wooden box to reduce heat loss.

Measurement accuracies of the power transducer and mass flow meter were 0.1 and 0.2% of full scale, respectively. The RTD probes were calibrated and accurate to within American Society of Heating, Refrigerating, and Air-Conditioning Engineers (ASHRAE) standards ($\pm 0.05^{\circ}$C),[21] over a temperature range of 0 to 50°C. The accuracy of these instruments was carefully examined to minimize measurement error, especially for the flow meter and RTD probes, due to the importance of these measurements in the calculation of heat transport. The combination of instrumentation used here resulted in an overall uncertainty of 0.11% in the heat input, 0.28% in the heat rejected, and 0.75% in the surface temperature measurement.

### C. Experimental Procedures

The RLHP was charged with 81 g of ammonia, which, when converted to a volume fraction, defined as the ratio to a total internal volume of 164 cm$^3$, was estimated to be 0.81–0.89. This charge was calculated using a liquid density of 610 and 550 g/l, corresponding to 20 and 55°C, respectively.[22,23] Compared to the volume fraction of conventional heat pipes, this relatively large value is necessary because the wick is located in both the evaporator and the condenser and the two large compensation chambers. Decreasing the charge to a value slightly less than 81 g increases the maximum heat transport, but will increase the minimum heat load for which reliable startup can be ensured. As a result, although it is important to ensure that there is sufficient charge to ensure startup, excess charge degrades the performance because the effective surface for condensing is reduced.

Varying the heat input ($q_i$, W) and cooling intensity ($mcp = \dot{m}_{C_{pc}}$, W/°C), the transient response characteristics and steady-state performance were evaluated in a gravitational environment with no tilt. Before beginning the measurements, the coolant temperature was regulated at 10°C, at which time the test protocol was initialized. The cooling intensity was then regulated to 72 or 290 W/°C by adjusting the valve installed just downstream of the mass flow meter, as shown in Fig. 3. When the temperature variations of the

evaporator and condenser were constant and within ±0.1°C, the heater power was increased in a stepwise fashion in 120-W increments to 1200 W. The heat input was increased to the next step, when the RLHP reached a steady-state condition defined when temperature variations of both the evaporator (or condenser) and the coolant were less than 0.1 and 0.05°C, respectively. This procedure was repeated in each step until the average evaporator or condenser temperature started to abruptly increase at the dryout limit where heat input exceeded the heat transport limit.

The average evaporator and condenser temperatures ($T_{e,m}$ and $T_{c,m}$) were calculated from the three surface temperatures as

$$T_{e,m} = (T_1 + T_2 + T_4)/3 \tag{1}$$

$$T_{c,m} = (T_6 + T_8 + T_9)/3 \tag{2}$$

The cooling intensity, $mcp$, was determined by the product of mass flow rate (kilograms per second) and coolant specific heat (J/kg · °C). The mass flow rate was calculated by the analog output, $V_m$:

$$\dot{m} = (2.5/60)(V_m - 1) \tag{3}$$

where $V_m$ ranged from 1 to 5 V and was linearly scaled to the mass flow rate varying from 0 to 10 kg/min. The coolant specific heat, $c_{p,c}$, was determined by the interpolation of the values provided by ASHRAE.[24] For 34% ethylene glycol, the specific heat varied linearly from 2300 to 2600 (J/kg · °C) as the coolant temperature changed from −10 to 40°C:

$$c_{p,c} = (300/50)(T_c + 10) + 2300 \tag{4}$$

The heat input ($q_i$, W) was calculated by the analog output $V_h$, which ranged from 1 to 5 V as the heat input changed from 0 to 1200 W:

$$q_i = (1200/4)(V_h - 1) \tag{5}$$

The heat transport ($q_t$, W) was determined by the product of $mcp$ and the temperature difference across the inlet and outlet of the cooling jacket:

$$q_t = mcp \times (T_{co} - T_{ci}) \tag{6}$$

The overall thermal resistance was estimated as

$$R_t = q_t/T_{e,m} - T_{c,m} \tag{7}$$

## III. Results and Discussion

### A. Thermal Analysis

Like many other moderate temperature heat pipes, the maximum heat transport is governed by the capillary limit criterion; that is, the capillary pumping pressure estimated from Eq. (8) must be greater than the total system pressure drop, as shown in Eq. (9):

$$\Delta P_c = 2\sigma/r_e \tag{8}$$

$$\Delta P_c \geq \Delta P_{L,v} + \Delta P_{L,j} + \Delta P_{\text{cond}} + \Delta P_{\text{eva}} \tag{9}$$

The right-hand side of Eq. (9) is the total system pressure drop, which consists of the pressure drops in the vapor and liquid lines, the condenser, and the evaporator. Among these, the frictional pressure drop in the liquid line is the dominant term when comparing the order of magnitude of individual terms. According to Kaya and Hoang,[5] the total system pressure drop for the given heat input, 300 W, is estimated to be approximately 2700 Pa. In the study, the working fluid was ammonia and a sintered metal wick with a pore size of 1.2 $\mu$m was used. Although the total system pressure changes with different configurations of the flow path, the estimated value can show the order of magnitude of the pressure drop for the present study. Using Eq. (9), the capillary pumping pressure for the present RLHP is calculated to be 36 kPa, which is much larger than the estimated total system pressure.

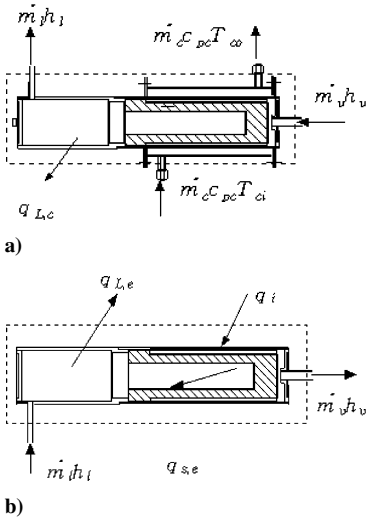


**Fig. 4 Heat balance in an RLHP a) condenser and b) evaporator.**

It is necessary to examine the energy conservation equations corresponding to the particular region comprising the evaporator and condenser to fully understand the operating characteristics of RLHP. Considering all the heat flows shown Fig. 4a, a heat balance equation for the condenser can be written as

$$\dot{m}_v h_v - \dot{m}_l h_l = \dot{m}_c c_{\text{pc}} T_{\text{co}} - \dot{m}_c c_{\text{pc}} T_{\text{ci}} + q_{L,c} + q_{s,c} + E_{\text{st},c} \tag{10}$$

where $E_{\text{st},c}$ and $q_{L,c}$ indicate the energy storage rate (W) inside the condenser and the heat loss (W) from the condenser, respectively. The term $q_{s,c}$ is the sensible heat transfer between the subcooled liquid and the condenser wall and can be expressed as[11]

$$q_{s,c} = A_c h_c (T_l - T_{w,c}) \tag{11}$$

The first two terms on the right-hand side of Eq. (10) indicate the amount of heat transport, which is determined by the coolant temperature difference as

$$q_t = \dot{m}_c c_{\text{pc}} T_{\text{co}} - \dot{m}_c c_{\text{pc}} T_{\text{ci}}$$

In the same way, the heat balance equation for the evaporator is

$$\dot{m}_v h_v - \dot{m}_l h_l = q_i - q_{L,e} - q_{s,e} - E_{\text{St},e} \tag{12}$$

where $q_{s,e}$ indicates the sensible heating required to heat the subcooled liquid to the saturation temperature:

$$q_{s,e} = \dot{m}(T_s - T_l) \tag{13}$$

In other words, $q_{s,e}$ can be estimated by the heat leakage transferred by condition, from the high-pressure to the low-pressure sides[5]:

$$q_{s,e} = \frac{2\pi k_{\text{eff}} L_w}{ln(d_{\text{wo}}/d_{\text{wi}})} \Delta T_w \tag{14}$$

where the temperature difference across the wick can be determined using the Clausius–Clapeyron equation,

$$\Delta T_w = \left(\frac{\partial T}{\partial P}\right)_{\text{sat}} (\Delta P_{\text{tot}} - \Delta P_w) \tag{15}$$

The term $\Delta P_{\text{tot}}$ represents the total system pressure on the right-hand side of Eq. (9). Using the effective thermal conductivity equation proposed by Dunn and Reay,[17] an approximate value of the heat leakage, $q_{s,e}$, was calculated as 28 W, if the term $\Delta P_{\text{tot}} - \Delta P_w$ is assumed to be equal to $\Delta P_c$ as defined by Eq. (8). This calculation was made at a temperature of 43°C for the configuration shown in Fig. 1. Also, the temperature difference across the wick, $\Delta T_w$, was estimated to be 0.6°C using Eq. (15).

Eliminating the term $\dot{m}_v h_v - \dot{m}_l h_l$ yields

$$q_t = q_i - (q_{L,e} + q_{L,c}) - (q_{s,e} + q_{s,c}) - (E_{\mathrm{st},e} + E_{\mathrm{st},c}) \quad (16)$$

Dividing both sides of Eq. (10) by $q_i$ gives

$$q_t/q_i = 1 - (q_{L,e} + q_{L,c})/q_i - (q_{s,e} + q_{s,c})/q_i - (E_{\mathrm{st},e} + E_{\mathrm{st},c})/q_i \quad (17)$$

The ratio of the heat transport to heat input is dependent on the heat loss, the sensible heat transfer, and the energy storage rate experienced in the evaporator as well as the condenser. Because there is no energy accumulation at steady state, the ratio can be determined by the heat loss and the sensible heat transfer. However, such a perfect steady state is seldom observed in LHPs because of the temperature fluctuations or hysteresis, which become more significant as the heat load decreases.

### B. Transient Response Characteristics

The transient operating characteristics of conventional LHPs are not well understood and several issues, including the aforementioned temperature hysteresis and related instabilities, require additional investigation. This is particularly true of the transient characteristics of RLHPs, which are even more complicated due to the disappearance of the thermal diode effect, because the condenser has the same wick structure as the evaporator. If the evaporator and condenser have the same radius of curvature, there may be an absence of any capillary pumping pressure or driving force to circulate the fluid though the loop. This phenomenon becomes more dominant in startup, when the wick in the condenser is also fully saturated with liquid, but becomes less significant as the heat input increases. When the vapor pressure becomes high enough to force the liquid front to recede into the compensation chamber, then the counteracting capillary pressure generated by the wick in the condenser disappears, as noted earlier.

For a given cooling intensity ($mcp$, W) and heat input ($q_i$, W), the transient variations of both the average evaporator and condenser temperatures can be represented as a function of time, as shown in Fig. 5. Overall, the average temperatures tend to quickly increase with increases in heat input and approach constant values for a given heat input, except when the dryout point has been reached, where the temperature difference disappears. After startup, the case of high cooling intensity resulted in a temperature 1.5–2.5°C higher than the liquid as the operation approached steady state. The difference approaches a smaller value of 1–1.5°C when the degree of cooling intensity decreases from 290 to 72 W/°C. This is reasonable if the larger temperature difference is caused by the simultaneous increases in the degrees of subcooling and superheat generated in the condenser and evaporator, respectively. In addition, the temperature difference during startup (e.g., 120 W) becomes 1–2°C larger than that observed in steady state, regardless of the level of cooling intensity. As noted earlier, for reliable startup, there must be

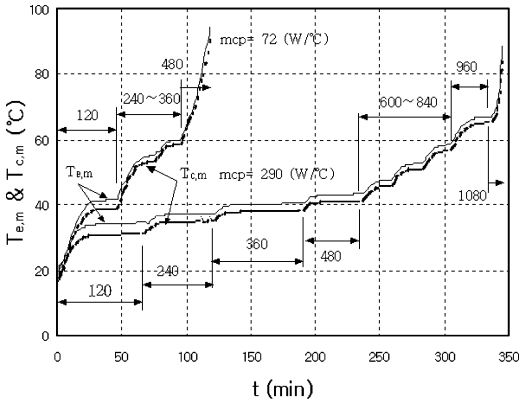


**Fig. 5 Variation of evaporator and condenser mean temperature as a function of time for a given cooling intensity and heater power.**

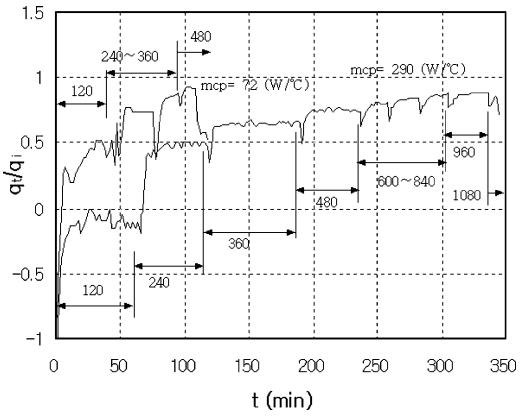


**Fig. 6 Variation of the ratio of heat transport to heater power as a function of time for a given cooling intensity and heater power.**

a sufficient temperature difference or level of superheat to provide the pressure difference required for the circulation of the working fluid.[5,11]

As indicated, the average evaporator temperature is approximately 40°C for a heat input of 360 W and a cooling intensity of 290 W/°C and increases to 60°C for the same heat input as the cooling intensity is reduced to a value of 72 W/°C. This implies that the RLHP operation is strongly influenced by the degree of cooling intensity, which is usually difficult to estimate, especially for the heat sinks used in space applications. The heat transport limit is defined as the maximum heat transport prior to reaching dryout, as indicated by an abrupt increase in the average temperature with simultaneous decreases in the heat transport. Thus, dryout corresponding to a cooling intensity of 72 W/°C begins near a point where the heat input and the average evaporator temperature are 480 W and 72°C, respectively. However, as illustrated in Fig. 5, dryout is significantly retarded for the case of high cooling intensity, 290 W/°C, and occurs at a heat input of 1080 W for nearly the same evaporator temperature.

In Fig. 6, the heat transport ratio for a given cooling intensity is presented as a function of time to analyze the transient response characteristics. Overall, both curves indicate that the heat transport ratios quickly increase with increases in heat input and approach certain values at which the heat transport ratio becomes constant for a given heat input until the dryout point is reached, where the transport ratios fall sharply. As shown, the lower cooling intensity provides higher heat transport ratio. For the same heat input of 360 W, the heat transport ratio is estimated to be 0.65 for a high cooling intensity of 290 W/°C but becomes approximately 0.9 for a cooling intensity of 72 W/°C. Regardless of the degree of cooling intensity, both heat transport ratios steadily increase from 0.5 to 0.9 as the heat input is increased from 240 W to the values corresponding to dryout. However, significantly different values are observed during the startup period, where the heat input is only 120 W. Here, the heat transport ratio reaches 0.5 for the low cooling intensity, 72 W/°C, whereas a negative value (approximately $-0.1$) is observed for the case of high cooling intensity. Again, this implies that the startup characteristics of the RLHP are heavily influenced by the degree of cooling intensity. Although a higher cooling intensity may offer greater heat transport, it results in a penalty during startup. This may be true for heat pipes in general, but is more distinct in the low heat load range, particularly for the current RLHP that has a long transport length and a condenser that generates the same capillary suction pressure as the evaporator.

This phenomenon needs to be explained in connection with the heat balance in the evaporator and condenser, as shown in Fig. 4 and Eq. (17). As shown, the heat transport ratio is greatly influenced by the sum of the three terms on the right-hand side of Eq. (17), which includes the heat loss, $(q_{L,e} + q_{L,c})/q_i$, the sensible heat transfer, $(q_{s,e} + q_{s,c})/q_i$, and the energy storage rate, $(E_{\mathrm{st},e} + E_{\mathrm{st},c})/q_i$, experienced in the condenser as well as in the evaporator. In the startup period, the contribution of the two terms, the heat loss and energy

storing terms, becomes more dominant, as indicated in previous investigations.[1,5] The heat loss term may be somewhat less than 1% at 1000 W, but may approach as high as 10% at 100 W. Furthermore, the energy storage rate represents another factor that reduces the heat transport. Existence of this loss can be verified by the fluctuations of the heat transport ratio in the startup period, which is coincident with the temperature hysteresis mentioned by Kaya and Hoang.[5] This phenomenon becomes more distinct as the cooling intensity increases and may explain why the low-cooling-intensity case shows a larger heat transport ratio, despite the greater heat loss during startup, as shown in Fig. 6.

These phenomena can also be interpreted from the perspective of the heat and mass transfer occurring in the RLHP. As the heat input decreases, it may be more difficult for the vapor to flow through the vapor line and to reach the condenser and so both the temperature and the heat transport ratio fluctuate with large amplitudes. In this case, the subcooled liquid in the condenser is pumped through the liquid line and is accumulated in the compensation chamber of the evaporator. Thus, the energy of the condenser decreases, particularly in the active zone where the amount of heat transport was measured, because the heat energy delivered by the vapor is insufficient to compensate for the energy loss, due to the liquid flowing out. Eventually, this may lead to the negative values of the heat transport ratio during startup. The negative values of heat transport can be seen not only in the startup period but also in the initialization process with no heat input. For the case of high cooling intensity, 290 W/°C, the coolant outlet temperature is 0.4°C lower than the inlet temperature. This shows that there exists an offset of 116 W in the heat transport. Finally, all of these may cause the heat transport ratio to be negative during startup for the case of high cooling intensity.

If the heat input is subsequently increased to 240 W, startup becomes more reliable and the heat transport ratio abruptly increases up to 0.5. The individual contribution of the three terms may change as the RLHP operation approaches a more stabilized condition. The heat loss and energy storage rate become less significant with increases in the heat load. This indicates that the heat transport ratio at steady state is governed primarily by the second term, the sensible heat transfer rate, which indicates heat leakage. The amount of heat leakage depends on the sensible heat transfer between the heating/cooling active zones and the compensation chambers. This heat leakage is expected to increase with increases in the degree of subcooling, which is required for operation of the LHP. The sensible heat transfer in the evaporator, $q_{s,e}$, was calculated to be 28 W when the temperature difference across the wick, $\Delta T_w$, was 0.8°C. In reality, the sensible heat transfer could be two or three times greater than this value, because the approximate value of the temperature difference corresponds to the temperature differences observed during steady state, as shown in Fig. 5. This estimation implies that the sensible heat transfer term becomes greater and may increase as the degree of subcooling increases. Another factor to be considered is the sensible heat transfer between the subcooled liquid and the condenser wall. Dickey and Peterson[11] proposed a theoretical model to estimate the amount of sensible heat transfer in the condenser using a shape factor analysis, but this is not suitable for the present study because the condenser wall temperature is a strong function of geometry.

### C. Performance Analysis

For a given cooling intensity and heat input, the average temperatures of the evaporator and condenser, as well as the coolant temperature difference, approach steady-state values as time increases. The relationship between the average evaporator temperature and heat transport (or heat transport ratio) was examined to investigate the heat transport limit of the RLHP. Also, the overall thermal resistance was analyzed to evaluate the quality of the RLHP when compared to conventional heat pipes.

As shown in Fig. 7, the average evaporator temperature can be represented as a function of heat transport for the two different cooling intensities. The current results obtained for the two different cooling intensities are compared with the results of the previous investigations conducted by Kaya and Hoang.[5] The curves

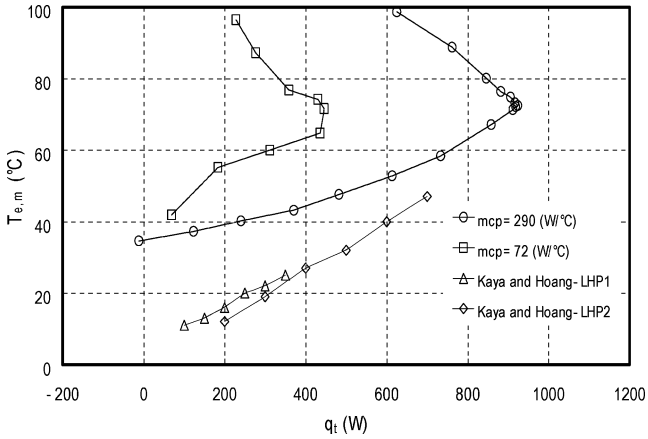


**Fig. 7 Variation of the mean evaporator temperature as a function of heater power for a given cooling intensity.**

obtained for LHP1 and LHP2 indicate lower operating temperatures for the same heat transport, which may be caused by several factors. LHP1 has nearly the same shape, but a total length of half of the present RLHP, whereas LHP2 has an equivalent overall length, but the evaporator length is doubled. Another factor may be the degree of cooling intensity, which was not clearly indicated in the previous investigation.

In the current investigation, the evaporator temperatures increase nearly linearly as the heat transport increases, up to a certain point. Beyond this point, the two curves show identical increases in the temperature rise, followed by a rapid reduction in the total heat transport. These inflection points clearly indicate the heat transport limits, and the evaporator temperatures corresponded to the dryout states, where the capillary pumping pressure becomes less than the total pressure drop and the capillary limit has been exceeded. For the case of the lower cooling intensity, 72 W/°C, the figure shows that the heat transport limit is 446 W and corresponds with an evaporator temperature of 72°C, whereas the heat transport limit is extended to a value of 924 W for nearly the same evaporator temperature as the cooling intensity increases to 290 W/°C. This behavior indicates that the degree of cooling intensity is a strong factor in the determination of the heat transport capability of these devices.

As pointed out earlier, the cooling method utilized in the condensers of these devices may be a dominant factor in governing the heat transport capacity, especially when applied to thermal control devices in spacecraft. One particular problem expected at low cooling intensities is the excessive rise in internal pressure. This becomes more important when using a working fluid with a high $dP/dT$, such as ammonia. Even at moderate heat loads, such as 400 W, these devices may still be susceptible to heat transport limitations followed by rapid increases in temperature, causing the internal pressure to exceed the allowable pressure limit. The saturation pressure corresponding to the temperature limit of 72°C is estimated to be 3.7 MPa. The most effective way to solve this problem will be to carefully control the operating temperature within a specified range to guarantee both performance and durability.

The heat transport ratio for the given heat input and cooling intensity is presented as a function of average evaporator temperature in Fig. 8. As indicated earlier, the behavior of a negative heat transport ratio is clearly indicated by the fact that the heat transport ratio remains negative during startup for a heat load of 120 W when using a high cooling intensity of 290 W/°C. During this time, the heat load is so low that it cannot provide reliable startup, as shown in Fig. 8. As indicated by the experimental results, the minimum heat load must be greater than 240 W to satisfy this requirement. In other words, the average evaporator temperature must be increased to a value of 35°C for a matched heat transport ratio such as 0.5, which was adopted as a reference value in this study to evaluate startup the reliability. However, the data for the high cooling intensity shows that the heat transport ratio increases rapidly immediately after the startup period and then steadily approaches a value of 0.9 as the

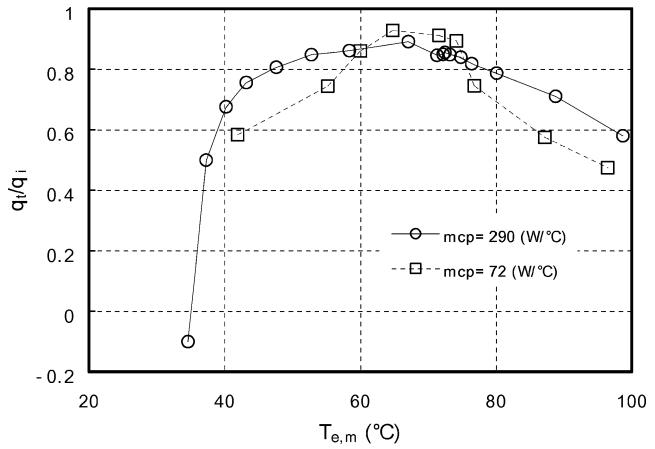


**Fig. 8 Variation of the ratio of heat transport to heater power as a function of the mean evaporator temperature for a given cooling intensity.**

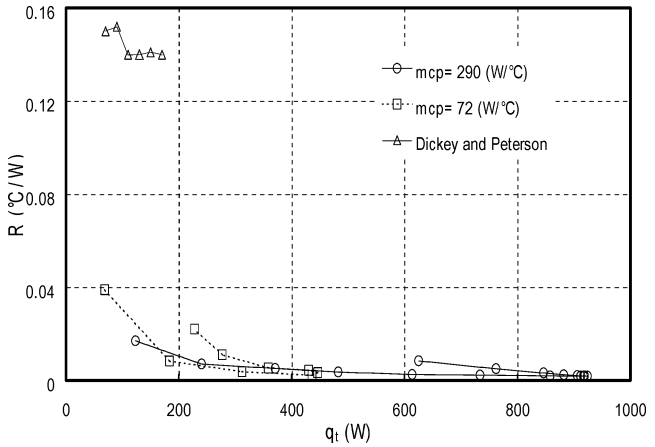


**Fig. 9 Variation of overall thermal resistance as a function of the heat transport for a given cooling intensity.**

evaporator temperature researches a limiting value of 72°C, corresponding to dryout. The case of low cooling intensity indicates that there is no problem during startup where the heat transport ratio and evaporator temperature approached 0.6 and 42°C, respectively, even in a low level of heat input such as 120 W. Similarly, the heat transport ratio tends to increase up to a value of 0.92, where the evaporator temperature is nearly the same as for high cooling intensities. Based on these results, it is recommended that the average evaporator temperature be maintained between 35 and 60°C to guarantee reliable startup and a relatively high heat transport ratio.

Using Eq. (7), variations in the overall thermal resistance for a given cooling intensity are represented as a function of the heat transport ratio and were compared with Dickey and Peterson's study[11] as shown in Fig. 9. The overall thermal resistance measured using the test article designed by Maidanik et al.[10] shows much higher values than those of the present study. This is the result of variations in the diameters of the evaporator and condenser, which are approximately half of those used in the present RLHP, while the total length is one and half times longer. The data clearly indicate that the overall thermal resistance decreases with increases in the heat transport and then approaches the heat transport limit. Thereafter, thermal resistance tends to increase and instead the value of heat transport decreases. The curve corresponding to a low cooling intensity indicates that the overall thermal resistance becomes 0.04°C/W when the startup is completed with a heat input of 120 W. However, the overall thermal resistance begins to decrease with increases in the heat transport and finally approaches a value of 0.003°C/W. For the case of high cooling intensity, the trend is similar except during startup, where the overall thermal resistance cannot be defined because of the negative heat transport. In this high cooling intensity, the data show that the overall thermal resistance decreases and eventually approaches a value of 0.003°C/W as the heat transport approaches 924 W. There is only a slight change in the resistance, despite the variation of the heat transport over the range of 240 to 926 W. Overall, the thermal resistance is maintained below 0.02°C/W for both cases, except during the startup and dryout periods, as shown in Fig. 9. In addition, the minimum heat transport required to maintain the resistance below 0.02°C/W is shown to be 120 W, which corresponds to 240 W in the heat load. When the heat load is greater than 240 W, it is possible to maintain an overall thermal resistance below 0.02°C/W as well as to guarantee a reliable startup regardless of the cooling intensity. The minimum heat transport, 240 W, is regarded as another lower bound corresponding to the lower temperature, 40°C, which is recommended for proper operation, as shown in Figs. 8 and 9.

## IV. Conclusions

In this study, the transient response characteristics and steady-state performance of a newly designed RLHP was tested, and the dependence on the level of heat load and cooling intensity was analyzed by employing parameters such as the average evaporator temperature, the heat transport ratio, and the overall thermal resistance. The RLHP showed excellent transient and steady-state performance characteristics over a wide range of heat loads and cooling intensities, but did reveal startup problems, which can be successfully eliminated by regulating the average evaporator temperature for the particular operating conditions.

It was found that the transient and steady-state performances were significantly influenced by the degree of cooling intensity, which should be optimized to guarantee both reliable startup and high heat transport capability. A heat transport limit of 446 W was observed for a relatively low cooling intensity, 72 W/°C, but this limit was extended dramatically to 924 W by increasing the cooling intensity to 290 W/°C. Also, the overall thermal resistance was maintained lower than 0.02°C/W on the whole, except for startup and dryout periods.

During startup at very low heat loads, the RLHP operation became unstable as the cooling intensity increased. Thus, it is recommended that the average evaporator temperature should be maintained between 35 and 60°C to guarantee a reliable startup, a relatively high heat transport ratio, and effective operation. Further tests in a thermal vacuum environment are required to better understand the physical mechanisms that govern the operation of the RLHP.

## Acknowledgments

The authors acknowledge the contributions of Joon-Min Choi, Korea Aerospace Research Institute, and Y. F. Maidanik, the Institute of Thermal Physics, Ural Branch of the Russian Academy of Science, for their help and suggestions.

## References

[1]North, M., Sarraf, D., Rosenfeld, J., Maidanik, Y., and Vershinin, S., "High Heat Flux Loop Heat Pipes," Conf. 970115, American Institute of Physics, New York, 1997, pp. 561–566.

[2]Faghri, A., *Heat Pipe Science and Technology*, Taylor Francis, Washington, DC, 1995.

[3]Lashley, C., Krein, S., and Barcomb, P., "Deployable Radiators—A Multi-discipline Approach," Society of Automotive Engineers Technical Paper Series, Paper 981691, July 1998.

[4]Ku, J., and Yun, S., "A Prototype Heat Exchanger for the Capillary Pumped Loop Flight Experiment," AIAA Paper 92-2910, June 1992.

[5]Kaya, T., and Hoang, T. T., "Mathematical Modeling of Loop Heat Pipes and Experimental Validation," *Journal of Thermophysics and Heat Transfer*, Vol. 13, No. 3, 1999, pp. 314–320.

[6]Laub, J., and McGinness, H. D., "Recirculation of a Two-Phase Fluid by Thermal and Capillary Pumping," Jet Propulsion Lab., California Inst. of Technology, TR 32-196, Dec. 1961.

[7]McGinness, H. D., "Capillary Pumping for Closed-Cycle Gas Systems," Research Summary 36-10, Vol. 1, Jet Propulsion Lab., California Inst. of Technology, Sept. 1961, pp. 9–13.

[8]Stenger, F. J., "Experimental Feasibility Study of Water-Filled Capillary-Pumped Heat-Transfer Loop," NASA TM X-1310, Lewis Research Center, Cleveland, OH, Aug. 1966.

[9]Maidanik, Y., Vershinin, S., Kohlodov, V., and Dolgirev, J., "Heat Transfer Apparatus," U.S. Patent 4515209, 7 May 1985.

[10]Maidanik, Y., Fershtater, S., and Goncharov, K., "Capillary-Pumped Loop for the Systems of Thermo Regulation of Spacecraft," European Space Agency SP-324, Dec. 1991.

[11]Dickey, J. T., and Peterson, G. P., "An Experimental and Analytical Investigation of the Operational Characteristics of a Capillary Pumped Loop," *Journal of Thermophysics and Heat Transfer*, Vol. 8, No. 3, 1994, pp. 602–607.

[12]Ku, J., "Thermodynamic Aspect of Capillary Pumped Loop Operation," AIAA Paper 94-2059, June 1994.

[13]Wirsch, P. J., and Thomas, S. K., "Performance Characteristics of a Stainless Steel/Ammonia Loop Heat Pipe, *Journal of Thermophysics and Heat Transfer*, Vol. 10, No. 3, 1996, pp. 326–333.

[14]Gernert, N. J., Baldassarre, G. J., and Gottschlich, J. M., "Loop Heat Pipes for Avionics Thermal Control," Society of Automotive Engineers Technical Paper Series, Paper 961318, 1996.

[15]Bienert, W. B., "Loop Heat Pipe Flight Experiment," CP420, American Institute of Physics, New York, 1998, pp. 511–513.

[16]Wulz, H., and Embacher, E., "Capillary Pumped Loop for Space Applications: Experimental and Theoretical Studies on the Performance of Capillary Evaporator Designs, AIAA Paper 90-1739, 1990.

[17]Dunn, P., and Reay, D., *Heat Pipes*, 3rd ed., Pergamon, New York, 1982.

[18]Maidanik, Y., "Development of Advanced Loop Heat Pipes for Thermoregulation of Modern Spacecraft," Inst. of Thermal Physics, Ural Branch of Russia Academy of Science, ISTC1360-00, Moscow, 2003.

[19]Dupont, V., Joly, L., Miscevic, M., and Platel V., "Capillary Pumped Loop Startup: Effects of the Wick Fit on Boiling Incipience," *Journal of Thermophysics and Heat Transfer*, Vol. 17, No. 2, 2003, pp. 138–144.

[20]Carey, V. P., *Liquid Vapor Phase Change Phenomenon*, Hemisphere, New York, 1992.

[21]American Society of Heating, Refrigerating, and Air-Conditioning Engineers (ASHRAE), "Methods of Testing for Seasonal Efficiency of Unitary Air-Conditioners and Heat Pumps," ASHRAE Standard ANSI/ASHRAE, 116-1983, 1983.

[22]Daubert, T. E., and Danner, R. P., *Physical and Thermodynamic Properties of Pure Chemicals, Data Compilation*, Hemisphere, New York, 1981.

[23]Lide, R. L., and Kehiaian, H. V., *CRC Handbook of Thermophysical and Thermochemical Data*, CRC Press, London, 1994.

[24]ASHRAE, *Fundamentals Handbook*, ASHRAE, New York, 1985, Chap. 18, pp. 1–10.